



# Sorption of Some Rare Earth Elements from Acidic Solution onto Poly(acrylic acid–co-acrylamide/16, 16-dimethylheptadecan-1-amine) Composite

A. H. Ali<sup>1</sup> · G. A. Dakroury<sup>2</sup> · M. S. Hagag<sup>1</sup> · Sh. M. Abdo<sup>1</sup> · K. F. Allan<sup>2</sup>

Accepted: 17 August 2021 / Published online: 24 August 2021

© The Author(s), under exclusive licence to Springer Science+Business Media, LLC, part of Springer Nature 2021

## Abstract

In this study, Acrylic acid (AA), acrylamide (AM), and 16,16-dimethylheptadecan-1-amine (PJM-T) were copolymerized using gamma irradiation with <sup>60</sup>Co  $\gamma$ -rays at a dose of 25 KGy to form a novel composite; Poly(acrylic acid-co-acrylamide/16,16-dimethylheptadecan-1-amine P(AA-co-AM/PJM-T). P(AA-co-AM/PJM-T) is characterized by different physicochemical techniques and used as a sorbent for rare earth elements from monazite. The optimum pH for the sorption process at 25 °C is 4.5 and the equilibrium attained at 60 min. Different kinetics and isothermal models is applied. The maximum adsorption capacity is  $182.15 \pm 3.73$  mg g<sup>-1</sup> at 25 °C. The sorption reaction regulates a pseudo 2nd order mechanism and the process is spontaneous.

**Keywords** Polymer composites · Rare earth elements · Monazite · Sorption · Adsorption kinetics · Isotherm

## Introduction

During the last centuries, REE has gained considerable importance due to the valuable need for these elements and their compounds in several fields. The physical and chemical properties of REEs make it suitable for electric, optical, and metallurgical technological fields [1–3]. REEs could be used in special alloys, magnets, catalysts, electric applications [4, 5], nuclear technologies, communications systems [6–8], medical purposes, and agricultural application [9].

Many ores for REEs are; monazite, lanthanite, xenotime, bastnäsite, allanite, loparite and phosphate rocks [10]. Monazite could be a REE (PO<sub>4</sub>)<sup>3-</sup> that's frequently found with other valuable minerals like ilmenite, rutile, zircon and cassiterite. There are 2 steps during the recovery of the REEs from its monazite ore. The 1st step is the decomposition of the ore and purification of REE compounds. In the 2nd step, this compound is separated into individual REE products by liquid–liquid extraction and/or ion exchange.

Several methods such as; precipitation, ion exchange, coagulation, flocculation, liquid–liquid extraction [11], solid–phase extraction [12], ionic liquid extraction [13], biosorption, and classical adsorption on different sorbents have been used for separating different lanthanides from aqueous solutions. These chemical methods of separation rely up on the concentration of REEs. At higher REEs concentrations, precipitation as hydroxide or as oxalate is favourable. In addition to solvent extraction [12] is employed. At lower REEs concentrations, ion exchange resin [14], nano filtration membrane [15], synthetic composite, [16] and bio-adsorption [17] are strongly recommended.

Among them, the adsorption method is utilized in treatment of REEs solutions due to its multiple superiorities of easy operation, low cost, high availability, and favorable retention efficiency [18].

16, 16-Dimethylheptadecan-1-amine (Primene JM-T; a primary amine) is especially employed in REE retention by solvent extraction and/or ion exchange. This can be due to its unique physical and chemical properties, resistance to oxidation, Fluidity and low viscosity at different temperatures, color stability. Primene JM-T extracts negative or anionic species [19]. However; Primene JM-T is incredibly toxic to aquatic life and expensive. Thus, it is important to develop a novel sorbent to solve this defect.

✉ G. A. Dakroury  
dr\_gdakrory2010@yahoo.com

<sup>1</sup> Nuclear Materials Authority, Maadi, P.O 530, Cairo, Egypt

<sup>2</sup> Nuclear Chemistry Department, Hot Laboratories Centre, Egyptian Atomic Energy Authority, P.O. 13759, Cairo, Egypt

Advanced sorption materials [20–22] and organic sorbents [23–25] like poly acrylic acid P (AA) which is cheap and non toxic. P(AA) was studied by authors efficiently in the adsorption of heavy metals [26–29]. Furthermore, P(AA) encompasses a great potential for adsorbing REE ions owing to its accessible carboxylic groups [30]. Enhancement of the hydrophilic character of poly carboxylic acids groups by polymerization with other hydrophilic monomers like; maleic acid) SiO<sub>2</sub>/Al<sub>2</sub>O<sub>3</sub> for sorption of Cesium, [31] acrylamide as N-donor functional moieties is studied. Authors declare that N-donor compounds have good sorption behaviour [32].

However, there's a limitation in studying co-polymerization of Primene JM-T with hydrophilic polymers.

In the present paper; REEs are extracted from monazite ore by treatment with alkaline solution. Separation of REEs from (PO<sub>4</sub>)<sup>3-</sup> and then from the impurities by direct precipitation are performed. The rare earth cake is still impure; should undergo further purification processes. A novel composite poly (acrylic acid –co -acrylamide/16, 16-dimethylheptadecan-1-amine) composite was used for this purpose after optimization of the sorption affecting factors like; pH, contact time, concentration and resin concentration. The mechanism of the sorption reaction is proposed by applying different kinetic models; pseudo 1st order, pseudo 2nd order, Elvoich and intra-particle diffusion. Furthermore, four isothermal models; Langmuir, Freundlich, Flory–Huggins and Temkin isotherm is applied.

## Experimental

### Reagents and Methodology

All reagents used during this work were of analytical grade and used without further purification. Acrylic acid (AA) got from Elf Chem. Co., ATOFINA, and France. Acrylamide (AM) was supplied by Fuchen Chemical Co., Ltd., Tianjin, China. Methylene bis-acrylamide (MBA) was supplied from (Merck, Germany). 16, 16-dimethylheptadecan-1-amine (PJM-T) is purchased from Adwic.

Monazite concentrate (monazite content about 90%) is supplied by nuclear materials authority, Cairo-Egypt. Double distilled water was used for the preparation of the composite. Hydrochloric acid (HCl) and sodium hydroxide (NaOH) were supplied from ADWIC (Egypt) for pH—adjustment.

### Co-polymer Preparation

A general procedure for grafting copolymerization of Acrylic acid (AA) and Acrylamide (AM) with Methylene bis-acrylamide (MBA) as acrosslinker using gamma irradiation technique was conducted as follows: 10% of prepared

monomer composition (60 AA:40 AM) was dissolved in degassed, distilled water. Then added to the total solution, 0.5 mass % MBA as a cross linker and 2% PJM-T were added to the reaction mixture then shaken overnight in a glass tube. The mixture is stirred at 400 rpm at room temperature for 2 h and ultrasonically treated for 10 min, after that it was subjected to Co-60 gamma rays irradiation (25 kGy). The irradiated product (grafted copolymer) was cut into small pieces and washed by acetone for removal of excess of unreacted monomers, washed with double distilled water and dried in an oven at 60 °C to a constant weight and then ground to the desired mesh size (< 300 μm) and keep for further use.

Figure 1 is a schematic diagram summarizes the preparation of P(AA-co-AM/PJM-T) composite. 10 ml of PJM-T mixed with 30 ml AA and 20 g acrylamide, 2.5 g MBA in 500 ml deoxygenated water.

### Gamma Radiation

Radiation is a very convenient method for graft initiation. It has advantages compared to chemical method as it is more efficient, economical, wide applicability and easily prepared [33]. Gamma Irradiation was carried out using the Co-60 gamma cell. A cell of type yMC-20 (Russia) was used at the Cyclotron Project, Inshas site, Egypt. The monomers were exposed to a dose of gamma radiation 25 kGy. Gamma radiation leads to the formation of free radicals, so it acts as an initiator for the polymerization process. These free radicals are active sites that cross linked with other monomers to get the grafted copolymer.

### Predicted Mechanism for Polymerization Process

Possible mechanism reactions for the graft polymerization of P(AA-co-AM/PJM-T) in the presence of MBA as cross linker can be predicted as shown in Fig. 2 [34].

### Preparation of REEs Solutions

Monazite was digested by alkaline method (caustic soda) [35]. 15 g of the digested REEs hydroxide cake was dissolved carefully in 50 ml conc. HCl acid in water bath at 85 °C. The initial concentration of REEs solutions is 1608 mg l<sup>-1</sup> and different concentrations from REEs were prepared via dilution of the stock standard solution for all batches adsorption trials. The stock solution keep in dark glass bottle and pH is monitored and adjusted continuously using small amounts of NH<sub>3</sub> or HCl to avoid metal precipitation.

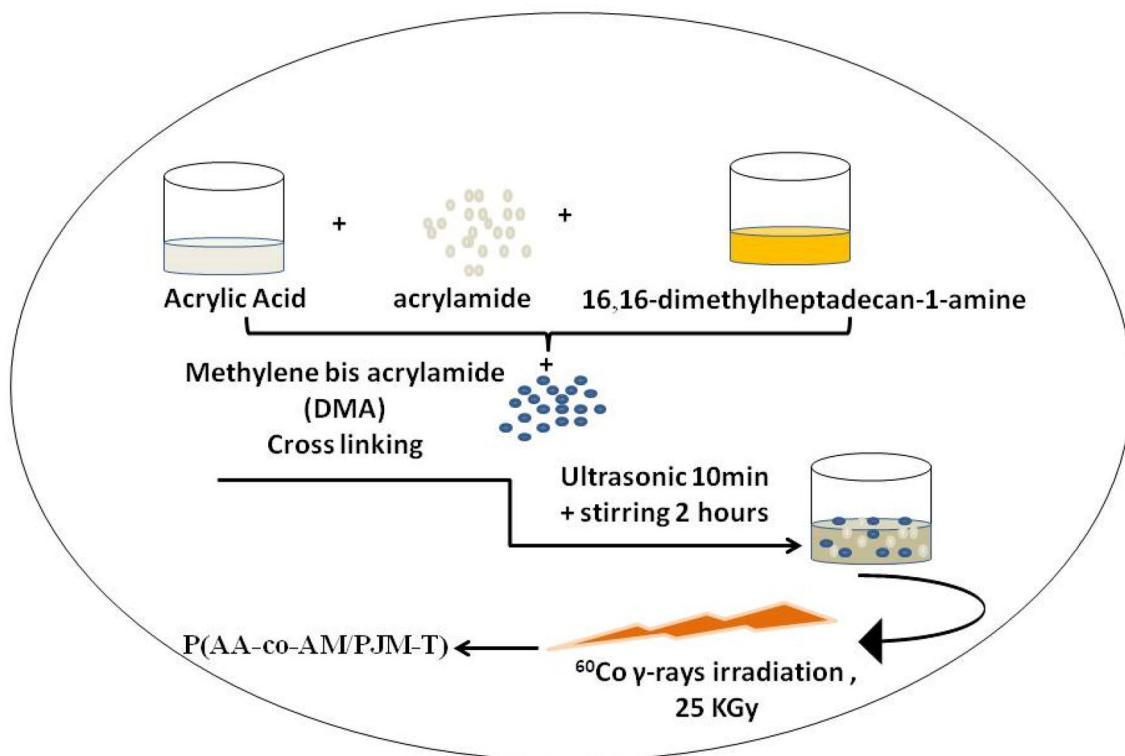


**Fig. 1** Schematic diagram for P(AA-co-AM/PJM-T) preparation

## Instruments

The surface morphology of the prepared composites was examined using a scanning electron microscope (JEOL JSM-5400, Japan). The FT-IR measurements were performed using a Bomem Micslon FT-IR spectrophotometer, model MB157, from Canada. Differential thermal and thermogravimetric analyses were carried out using Shimadzu DT-60, Japan. The Samples were exposed to temperature up to 800 °C with a heating rate of 20 °C min<sup>-1</sup> in the presence of nitrogen atmosphere to avoid thermal oxidation of the powder samples.. Shimadzu X-ray diffraction (XRD), model XD-D1, Kyoto, Japan, was used to investigate the crystalline structure, with a diffraction angle (2θ) within the range 4–70°. Pore size distribution and corresponding porosity calculated with the aid of pore-sizer chromatech 9320, USA. The concentration of REEs solutions is determined by Inductive Coupled Plasma Optical Emission Spectrometer (Prodig Axial high dispersion ICP-OES model, USA and UV- spectrophotometer (single beam multi-cells-positions model SP-8001).

## Point of Zero Charge

Point of zero charge ( $pH_{pzc}$ ) is that the pH at which the surface charge is zero [36]. The surface charge at pH lower

than ( $pH_{pzc}$ ) is positive and that at pH higher than ( $pH_{pzc}$ ) is negative. The small value of  $pH_{pzc}$  is considered as sign for an efficient sorbent because it gives a verity of pH for the sorption of cations.  $pH_{pzc}$  can be determined practically by adjusting pH for a series of flasks each one contains 0.5 g of the adsorbent with 20 ml of 0.01 M (NaCl) and the pH was adjusted from 1.0 to 7.0 ( $pH_{initial}$ ). The solution was shaken for 24 h and the final pH of the solutions was measured ( $pH_{final}$ ).  $pH_{pzc}$  is determined by plotting  $pH_{initial}$  against  $\Delta pH$  ( $pH_{final} - pH_{initial}$ ).

## Sorption Studies

Sorption studies were carried out onto P(AA-co-AM/PJM-T) using Egyptian high-grade monazite sample. Sorption parameters. i.e. pH (2–4.5), contact time (15–120), initial concentration (200–2000 mg l<sup>-1</sup>) and resin ratio (V/m) varied to select the best conditions for sorption. 0.1 g of the sorbent contacted with 20 ml of the adsorbate solution and after sorption time; samples were filtered and thus separated from the solution.

The Sorption efficiency of the REE ions at each interval of time is given by Eq. (1).

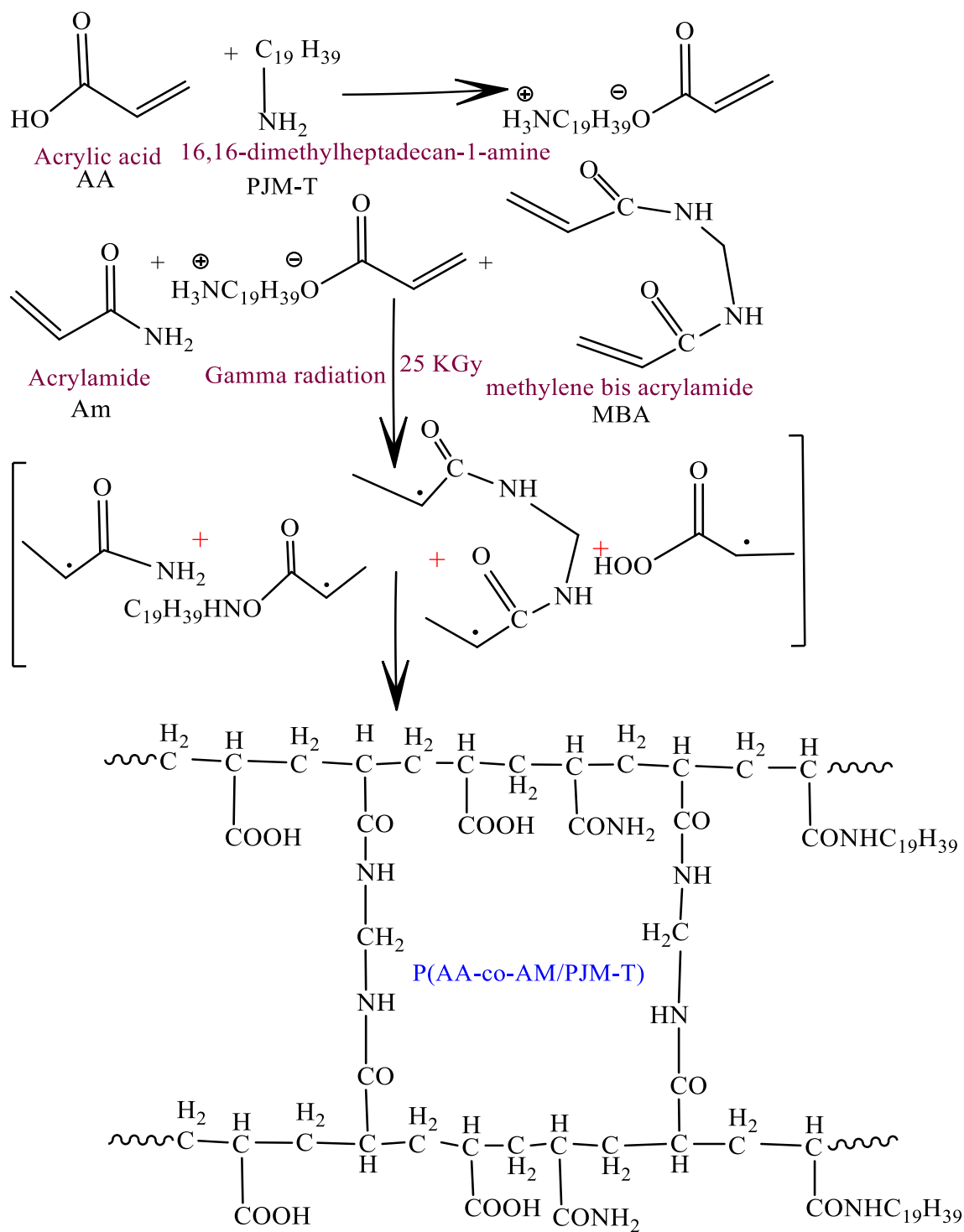


Fig. 2 Predicted mechanism for polymerization process

$$\text{Sorption efficiency (\%)} = \left( \frac{C_0 - C_f}{C_0} \right) \times 100 \quad (1)$$

Adsorbed amount  $q$  ( $\text{mg g}^{-1}$ ) is calculated using Eq. (2):

$$q = \left( \frac{C_0 - C_f}{C_0} \right) \times \frac{V}{m} \quad (2)$$

where  $q$ , is the amount sorbed ( $\text{mg g}^{-1}$ ).  $C_0$ ,  $C_f$  are the initial and final concentrations of the REE ions, respectively.  $m$  is the weight of the P(AA-co-AM/PJM-T) (g) and  $V$  is that the volume of solution (l).

### Kinetic Modeling

Kinetic modelling can give a proposal for the mechanism of the sorption reaction. Four kinetics models are applied through this study; Pseudo 1st order, pseudo 2nd order, Elovich model and intra-particle diffusion model.

#### Pseudo 1st Order & Pseudo 2nd Order Models

The pseudo-first order equation is given by Eq. (3) [37]

$$\text{Log}(q_e - q_t) = \log q_e - \frac{k_1}{2.303} t \quad (3)$$

where  $q_e$  and  $q_t$  are the sorbed amounts of REE ions; ( $\text{mg g}^{-1}$ ) at equilibrium time and at any time  $t$ , respectively;  $k_1$  ( $\text{min}^{-1}$ ) is the 1st order rate constant.

The pseudo-second order is given by the Eq. (4) [38]

$$\frac{t}{q_t} = \frac{1}{k_2 q_e^2} + \frac{1}{q_e} t \quad (4)$$

where  $k_2$  ( $\text{g mg}^{-1} \text{min}^{-1}$ ) is the 2nd order rate constant.

#### Elovich Model

It's applied for chemisorptions reaction and give by Eq. (5) [39]

$$q_t = \frac{1}{\beta} \ln(\alpha\beta) + \frac{1}{\beta} \ln t \quad (5)$$

where  $\alpha$  and  $\beta$  are the Elovich coefficients.  $\alpha$  ( $\text{mg g}^{-1} \text{min}^{-1}$ ) represents initial adsorption rate and  $\beta$  expressed desorption constant ( $\text{g mg}^{-1}$ ) during any experiment related to the activation energy involved in chemisorptions.

#### Intra- particle diffusion model

The intra-particle diffusion model is applied using Eq. (6) [40]

$$q_t = K_{id} t^{0.5} + C \quad (6)$$

where  $k_{id}$  is the intra-particle diffusion rate constant ( $\text{mg g}^{-1} \text{min}^{-1/2}$ ) and  $C$  is the intercept.

### Isotherm Modeling

Four isotherm models are applied through this study; Langmuir [41], Freundlich [42], Flory–Huggins [43] and Temkin isotherm [44].

#### Langmuir Model

By Eq. (7), Langmuir isothermes model could be applied

$$\frac{C_e}{q_t} = \frac{1}{bQ_0} + \frac{1}{Q_0} C_e \quad (7)$$

where  $Q_0$  is the Langmuir adsorption capacity ( $\text{mg g}^{-1}$ ),  $b$  is the constant related to free energy of sorption where  $\Delta G^0$  ( $b \propto e^{-\Delta G^0/RT}$ ) and  $C_e$  is the equilibrium concentration.

#### Freundlich Model

Freundlich model is illustrated by Linear Eq. (8)

$$\log q_e = \log K_f + \frac{1}{n} \log C_e \quad (8)$$

where,  $K_f$  is Freundlich constants and  $n$ , related to adsorption capacity and intensity.

#### Flory–Huggins Model

Flory–Huggins Eq. (9) and the linear relation is given by Eq. (10):

$$\frac{\theta}{C_o} = K_{FH} (1 - \theta)^{n_{FH}} \quad (9)$$

$$\log \frac{\theta}{C_o} = \log K_{FH} + n_{FH} \log(1 - \theta) \quad (10)$$

where,  $\theta = 1 - C_e/C_0$ , the degree of surface coverage,  $n_{FH}$  the number of occupied sites, and  $K_{FH}$ , the Flory Huggins equilibrium constant ( $\text{Lmol}^{-1}$ ). The equilibrium constant  $K_{FH}$  is used to know the spontaneity of  $\Delta G^0$  with the aid of Eq. (11):

$$\Delta G^0 = RT \ln K_{FH} \quad (11)$$

where  $\Delta G^0$  is the standard free energy,  $R$  is the universal gas constant,  $8.314 \text{ Jmol}^{-1} \text{ K}^{-1}$ , and  $T$  is temperature in Kelvin.

## Temkin Model

Temkin assumes a linear variation of the adsorption heat with the degree of overlap. The model is given by the Eqs. (12, 13) [44]

$$q_e = \frac{RT}{b_T} \ln(A_T C_e) \quad (12)$$

$$q_e = B_T \ln A_T + B_T \ln C_e \quad (13)$$

where:  $B_T = \frac{RT}{b_T}$ ,  $A_T$ ,  $b_T$  are constants,  $A_T$  ( $\text{L mol}^{-1}$ ) is related to the maximum binding energy,  $b_T$  is said to be the adsorption heat.

The loaded P(AA-co-AM/PJM-T) by REE was desorbed in several concentrations (0.01, 0.1, 0.5 and 1 M) of HCl as desorbing solution at room temperature for an hour. The mixture was filtrate to isolate the P(AA-co-AM/PJM-T) composite from the liquid phase, and then the concentration of REE ions measured. The desorption efficiency % was calculated using Eq. (14):

$$\text{Desorption\%} = \frac{C_{aq}}{C_s} \% \quad (14)$$

where  $C_{aq}$  is related to the concentration of REE within the aqueous phase,  $C_s$  is that the concentration of REE within the P (AA-co-AM/PJM-T) composite.

## Result and Discussion

### Characteristics of the Adsorbent

#### Adsorbent Morphology

The morphology for P(AA-co-AM/PJM-T) composite Fig. 3a shows a dense packed morphology with well definite

**Fig. 3** SEM of **a** P (AA-co-AM/PJM-T). **b** Loaded RE ions onto P(AA-co-AM/PJM-T) composite

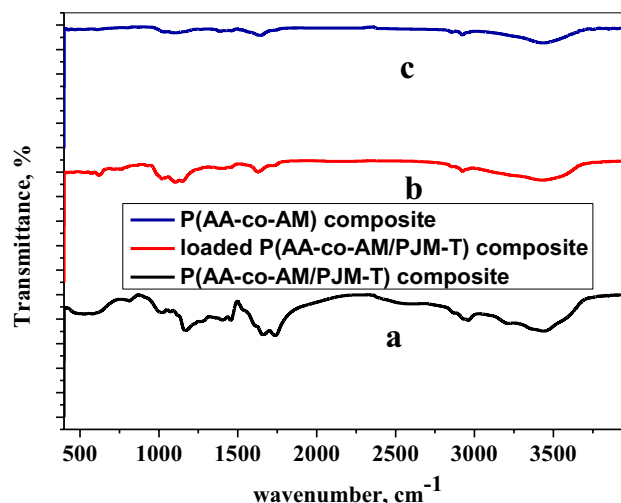
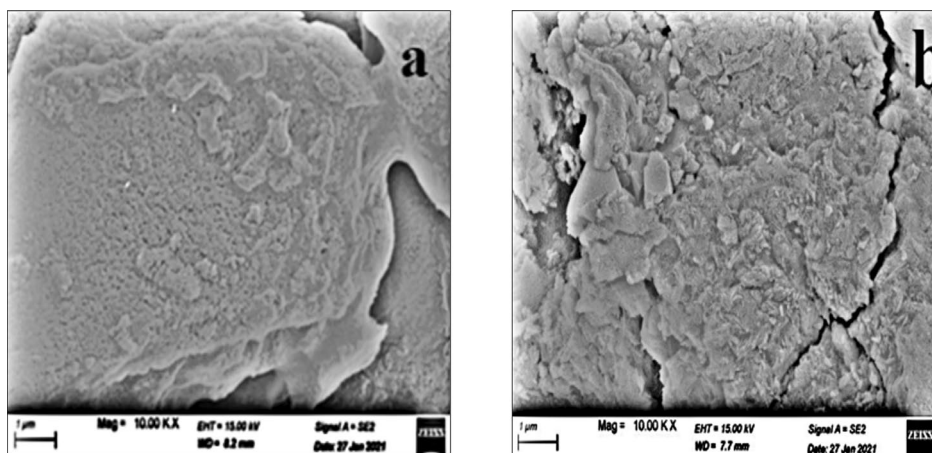


**Fig. 4** FT-IR spectrum of **a**-P(AA-co-AM/PJM-T) composite. **b**-Loaded P(AA-co-AM/PJM-T) with REES. **c**-P(AA-co-AM) composite

dimensions of the polymeric matrix. Sorption of rare earth ions onto P(AA-co-AM/PJM-T) (Fig. 3b) leads to fracture surface i.e. The smoothing of the surface decreases.

#### FT-IR Analysis

FT-IR analysis in Fig. 4a showed the characteristic absorption peaks for the functional groups of P(AA-co-AM/PJM-T) composite. The two broad absorption signals at  $3439 \text{ cm}^{-1}$  [45] and  $1641 \text{ cm}^{-1}$  were attributed to OH of AA. However, the absorption peak at  $3213 \text{ cm}^{-1}$  is assigned to NH for PJM-T and acrylamide. CH group is represented by the absorption peak at  $2960 \text{ cm}^{-1}$ . A peak at  $1735$  is assigned to C=O [45] while that at  $1456 \text{ cm}^{-1}$  belongs to stretching band of CN and  $1166 \text{ cm}^{-1}$  is another peak related to NH group [46]. The signal at  $1661 \text{ cm}^{-1}$  is the

characteristics (N–H) stretching peak [47]. Two existed signals at  $1078\text{--}1128\text{ cm}^{-1}$  are attributed to the 2nd stretch OH group. The peaks at range  $1166\text{--}811$  are due to C–H stretching of CHO group that at range  $579\text{--}525$  assigned to  $\text{CH}_2$  aliphatic compounds. For loaded P(AA-co-AM/PJM-T) with REEs in Fig. 4b; the intensity of bands of –OH and –NH decrease due the participating of these groups in the coordination of REEs. CO as well as CN bands are shifted to  $1732, 1407\text{ cm}^{-1}$ , respectively. In any cases, binding of REEs strongly affects the chemical environment of N–, OH– groups. Several bands in the range  $900\text{--}400$  related to

REEs-O stretching bands. Figure 4c for P(AA-co-AM), The broad and strong absorption band near  $3435\text{ cm}^{-1}$  represents the stretching vibration of –OH group in AA and -NH group in AM the peak at  $1646\text{ cm}^{-1}$  was the stretching vibration band of carbonyl group in AM. The  $1459\text{ cm}^{-1}$  is related to the stretching vibration of C–N bond in graft copolymer. The absorbance at  $2924.5\text{ cm}^{-1}$  is assigned to –C–H stretching of the acrylate unit.

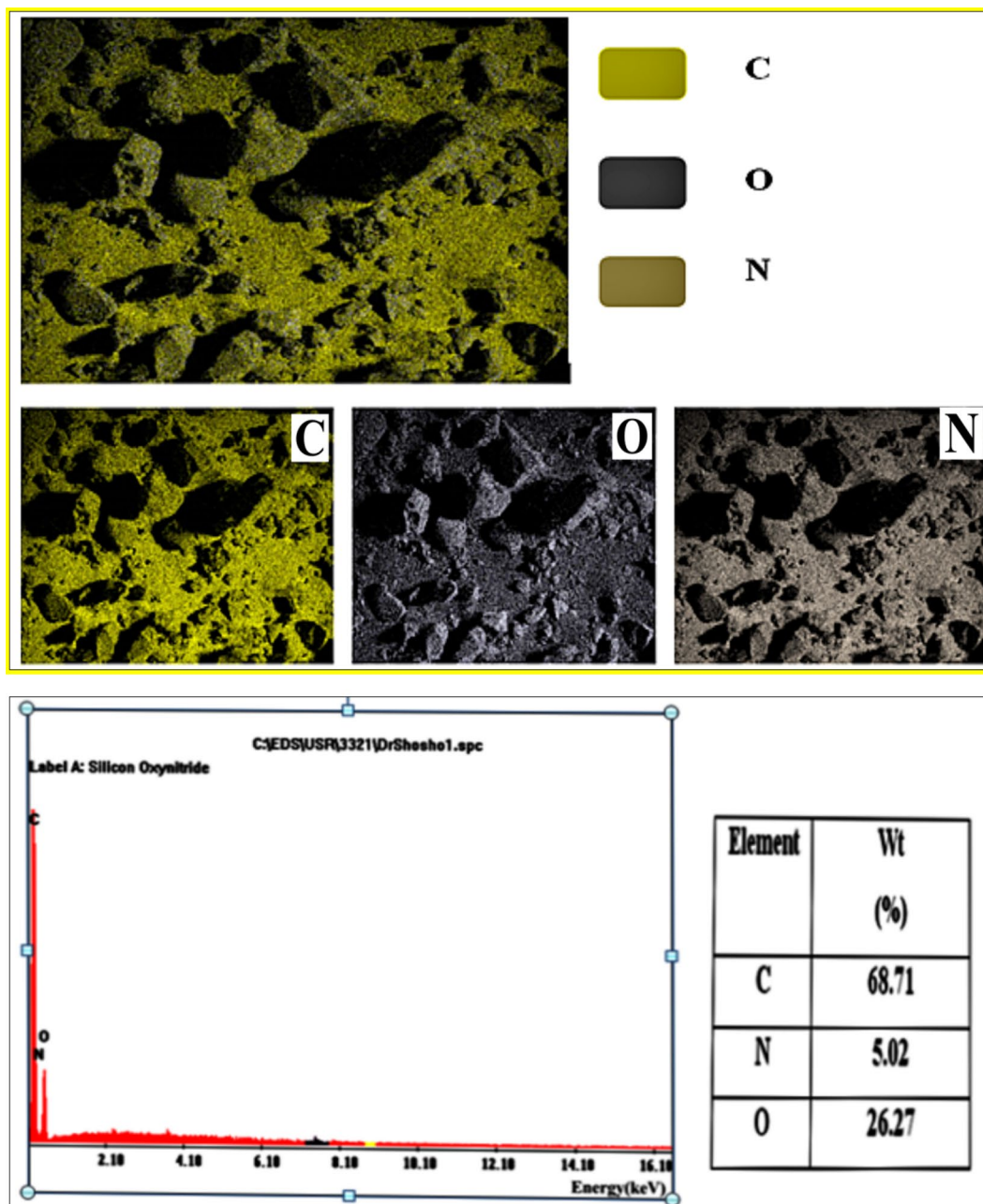


Fig. 5 EDX-mapping spectra of P(AA-co-AM/PJM-T) composite

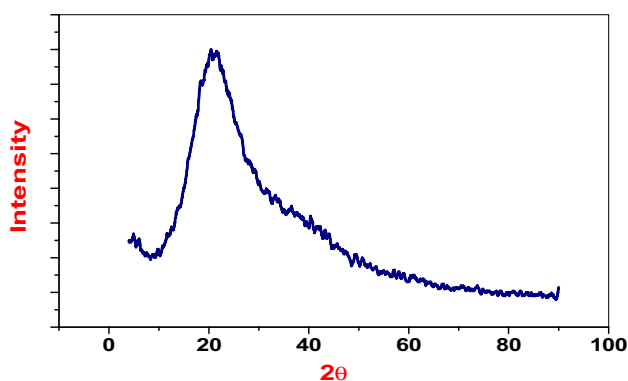


Fig. 6 X-ray diffraction of P(AA-co-AM/PJM-T) composite

### Energy Dispersive (EDX) Spectroscopy

The energy dispersive spectra of P(AA-co-AM/PJM-T) composite are shown in Fig. 5. The spectrum of the composite revealed an intense carbon band, oxygen and nitrogen bands due to the main constituents of acrylic acid chains, acrylamide and PJM-T of the copolymer. The composite has the highest percentage of carbon followed by nitrogen and oxygen.

### X-ray Diffraction Analysis

X ray diffraction may be a tool for recognition of the degree of crystalline of P(AA-co-AM/PJM-T) composite. Figure 6 clarify that P(AA-co-AM/PJM-T) is amorphous structure with non crystalline peak at  $2\theta = 20.4$  such as atactic structures of PAA [48].

### Thermogravimetric Analysis

Thermogravimetric analysis is depicted in Fig. 7a. The thermal stability of P(AA-co-AM/PJM-T) composite decrease because the temperature is raised and also the composite losses its weight in three decomposition steps. The 1st step starts from 170 °C to 222 °C with weight loss of 1.94%. This step accompanied by endothermic peak at 220 °C due to loss of adsorbed water. The second step starts at 340 °C with 42.3% weight loss. The endothermic peak at 340 °C attributed to loss of water from PAA and formation of poly acrylic acid anhydride [39]. Then the third step accelerated from 400 °C to 800 °C with 92.07% weight loss and can be ascribed to the degradation of composite. An exothermic peak at 528 °C because of burning of organic substances [49].

DSC provides qualitative and quantitative information to the thermal properties of P (AA-co-AM/PJM-T) such as the melting and degradation temperatures, glass transition temperature, melt and crystallization enthalpy, specific and latent heats, polymorphism, and purity of the materials. Figure 7b shows the DSC curve of PAA. As can be seen from this curve, there are an endothermic peak at 220 °C, at which the sample consumes energy values 304.6 J/g, respectively. In addition, the curve shows two exothermic peaks at 154.4 °C and 458 °C with emitted heat values of  $-81.71$  and  $-16.81$ , respectively. The endothermic peak at 220 °C due to water loss while the exothermic peak at 400 °C corresponds to degradation of composite. The first exothermic peak at 154.4 due to amorphous aggregate of the composite.

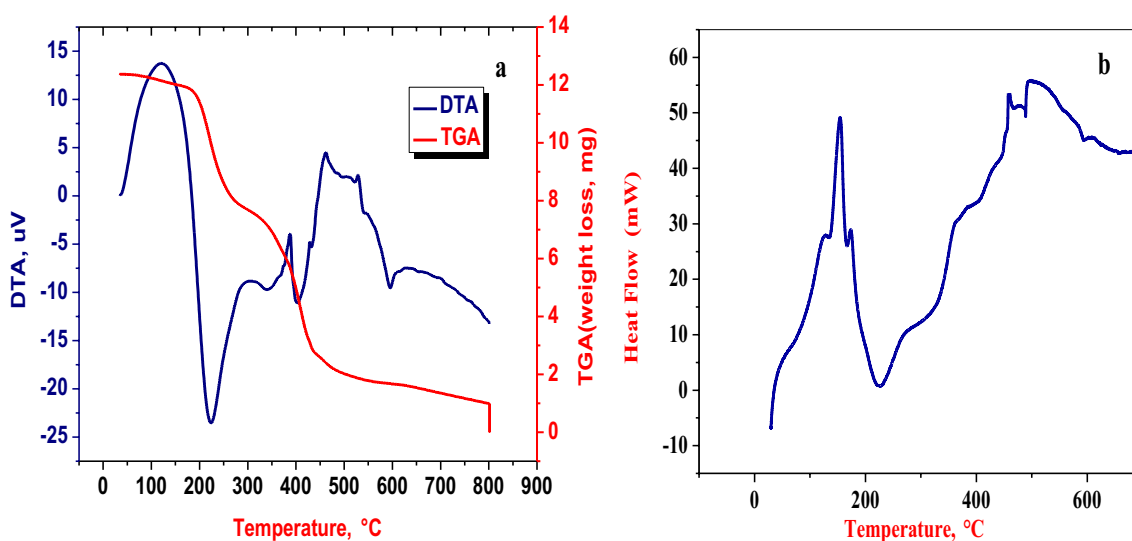
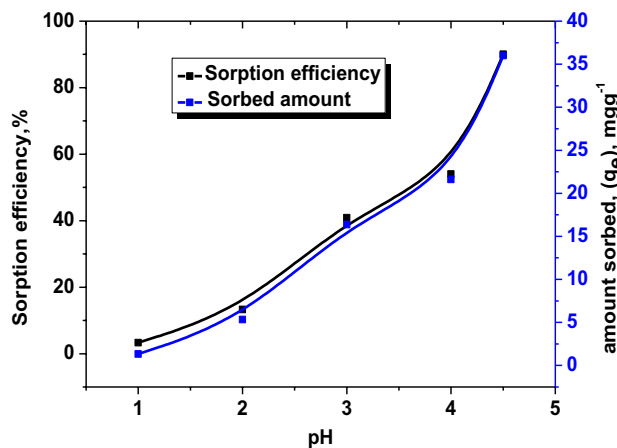


Fig. 7 a DTA-TGA analysis of P(AA-co-AM/PJM-T) composite. b DSC of P (AA-co-AM/PJM-T) composite



**Table 1** Total pore area and pore size analysis and the corresponding porosity of P(AA-co-AM/PJM-T) composite

Sorbent	Total pore area (m <sup>2</sup> g <sup>-1</sup> )	Average pore diameter (nm)	Bulk density (g mL <sup>-1</sup> )	Apparent density (g mL <sup>-1</sup> )	Porosity (%)
P(AA-co-AM/PJM-T)	8.53 ± 0.4265	119.4 ± 5.97	0.622 ± 0.0311	0.929 ± 0.0465	33.07

**Fig. 8** Amount sorbed of REEs onto P(AA-co-AM/PJM-T) composite at different pH at 25 °C

### Surface Characteristics

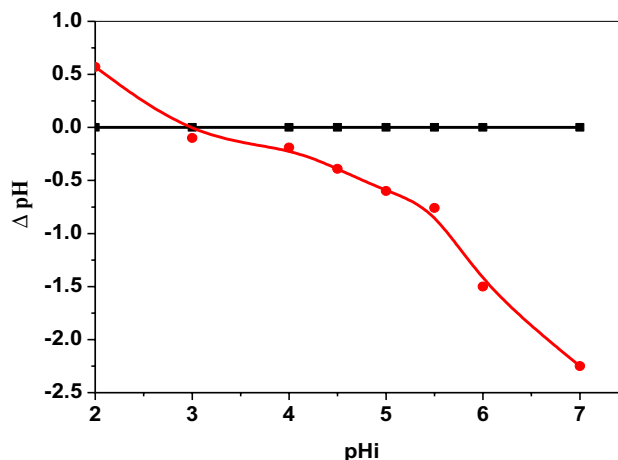
Surface characteristics of any sorbent give an indication for its efficiency for the sorption process. Total pore area includes macro, meso and micro pores. However, the average pore diameter is 119.4 nm (more than 50 nm) closely related to the presence of macropores. The presence of macropores responsible for the cracking of the surface. The difference between apparent density and bulk density is reasonable evidence for existence of open pores available for sorption process. The results for surface characteristics are listed in Table 1.

### Sorption Study

#### Effect of [H<sup>+</sup>] Concentration

The sorption process is extremely affected by the change in pH parameter due to ionization of surface functional groups. Different sorption experiment within pH range (2–4.5) performed to determine the optimum pH. Figure 8 represents the relation between amount sorbed ( $q_e$ ) and pH and it is obvious that as the pH increase; the sorbed amount increases. This is owing to the increase of the total net negative charges of the sorbent surface attracting metal ions and a less competition between H<sup>+</sup> and REE ions [50].

The  $pH_{ZPC}$  (pH of zero point charge) is an important physicochemical parameter depends on the surface chemistry of

**Fig. 9** Determination of  $pH_{ZPC}$  for P(AA-co-AM/PJM-T) composite

the sorbent. P(AA-co-AM/PJM-T) composite has a negative surface charge related to Acrylic acid. The pH of the point of zero charge of P(AA-co-AM/PJM-T) composite is 3 shown in Fig. 9; the charge of the surface is positive at pH < 3. At pH values above this given value, the electric charge of the adsorbent is (–ve) and can attract the REE ions (+ve). So, it's necessary to choose the working pH > 3.

The optimum pH is chosen at pH 4.5 due to formation of rare earth hydroxides precipitate at higher pH. This is confirmed by Hydra/Medusa chemical equilibrium software [51] starting with rare earth ions (III) concentration 200 mg l<sup>-1</sup>, 25 °C and different [H<sup>+</sup>] concentration (1–12). Figure 10 illustrates rare earth ions (III) predominate at pH up to 5. In Fig. 10a Ce(III), Nd(III), Sm(III) and Pr(III) are predominate species at pH < 6. At pH > 6, the predominate species are Ce(OH)<sub>3</sub>, Nd(OH)<sub>3</sub>, Sm(OH)<sub>3</sub>, Pr(OH)<sub>3</sub> and complex ions like Ce(OH)<sub>2</sub><sup>+</sup>, Ce(OH)<sub>2</sub><sup>+</sup>, Nd(OH)<sub>2</sub><sup>+</sup>, Nd(OH)<sub>2</sub><sup>+</sup>, Sm(OH)<sub>2</sub><sup>+</sup>, Sm(OH)<sub>2</sub><sup>+</sup>, Pr(OH)<sub>2</sub><sup>+</sup>, Pr(OH)<sub>2</sub><sup>+</sup> at pH > 10 the predominate species are Ce(OH)<sub>4</sub><sup>-</sup>, Sm(OH)<sub>4</sub><sup>-</sup>, Pr(OH)<sub>4</sub>.

The same in Fig. 10b; the predominate species are Eu(III), Gd(III), Dy(III), Tb(III) while the Lu(III) is predominate species at pH < 5 (Fig. 10c).

#### Effect of Contact Time

The effect of time on adsorption process studied at intervals (15–120 min) and represented in Fig. 11. The equilibrium time of the sorption reaction was reached rapidly at

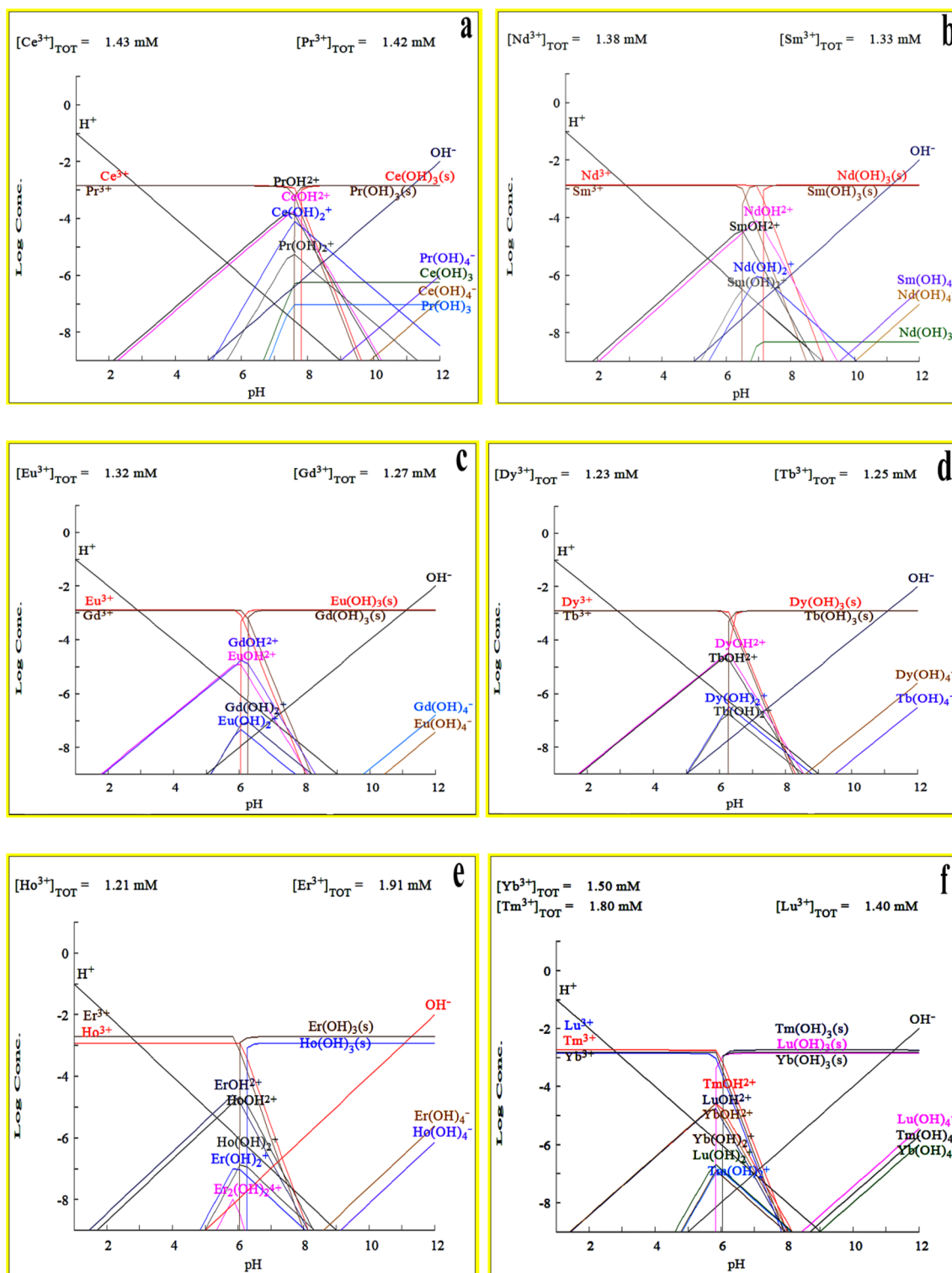
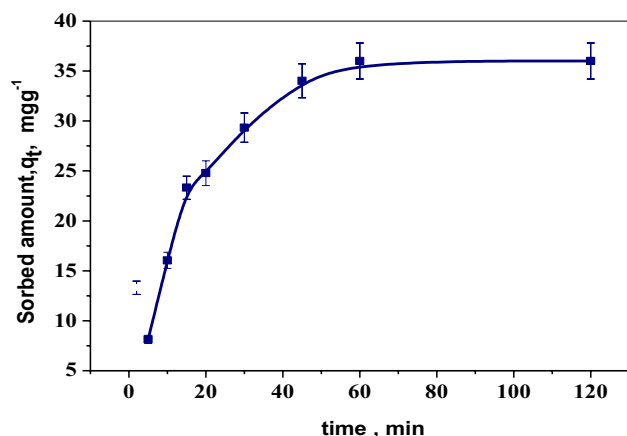
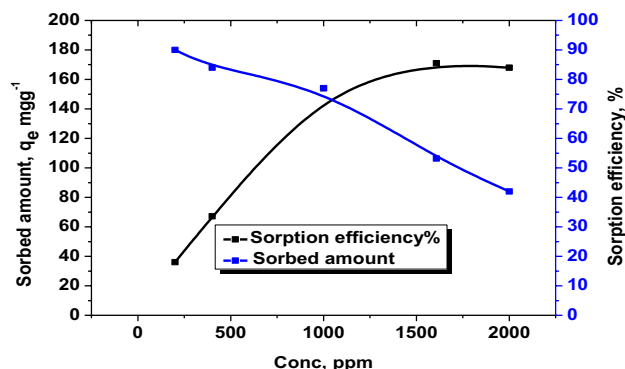


Fig. 10 Speciation diagrams for some rare earth ions at 25 °C



**Fig. 11** Sorption of rare earth ions onto P(AA-co-AM/PJM-T) at 25 °C and initial concentration 200 mg l<sup>-1</sup>



**Fig. 12** Sorption isotherm of rare earth ions onto P(AA-co-AM/PJM-T) at 25 °C

nearly an hour. The sorbed amount increases at time interval (15–60 min) due to the gradual occupancy of accessible sites on abundant availability of active sites on P(AA-co-AM/PJM-T) [52]. At 60 min, the equilibrium time, complete occupancy of the P(AA-co-AM/PJM-T). The optimum sorbed amount is 36 mgg<sup>-1</sup>.

#### Effect of Concentration

The effect of initial REE ions concentration on the sorbed amount is shown in Fig. 12. The concentrations in the range from 200 to 2000 ppm of the REE ions have been studied. The adsorbed amount ( $q_e$ ) of rare earth ions was found to decrease as the REE ions concentration increase. This is owing to P(AA-co-AM/PJM-T) as a sorbents have a fixed number of active sites and at higher concentrations of rare earth ions, the driving force to P(AA-co-AM/PJM-T) surface/liquid interface increases till the active sites become saturated [53, 54].

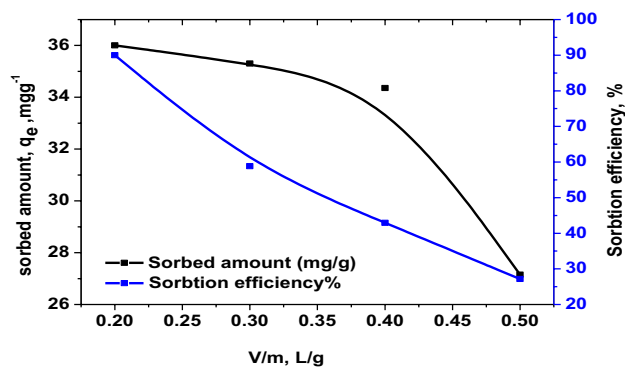


**Fig. 13** Effect of V/m on the sorption efficiency of rare earth ions onto P(AA-co-AM/PJM-T) at 25 °C

Four models of sorption: Langmuir, Freundlich, Flory–Huggins and Temkin, were applied to identify the fit model to adsorption reaction.

#### Effect of V/m Ratio

Impacted volume to weight ratio (V/m) on adsorption of RE ions was studied in the range from 0.2–0.5 Lg<sup>-1</sup> to evaluate the preferred volume/weight of sorbent for high uptake percentage. As present in Fig. 13, the uptake efficiency inversely related with V/m ratio. Thus, the best V/m ratio was chosen at 0.2.

#### Kinetic Modeling

##### Pseudo 1st –Order & Pseudo 2nd Order

The sorption reaction is more fitted with the kinetic model that has a highest correlation factor  $R^2$  and the  $q_{e(cal)}$  identity with  $q_{e(exp)}$ . Figure 14a, b illustrates the plots for pseudo 1st order fitting and pseudo 2nd order fitting. Table 2 lists the values of  $q_{e(exp)}$ ,  $k_1$  for pseudo 1st order,  $k_2$  for pseudo 2nd order and the correlation coefficient ( $R^2$ ) of the two models. From the result, pseudo 1st order plot shows a straight line with correlation factor  $R^2 = 0.987$  proposing that pseudo 1st order model is applicable. However,  $R^2$  for pseudo 2nd order plot is 0.999 which is more than that of pseudo 1st order. The calculated adsorption capacity is identical with the experimental one for both models. So, it's clear that, the sorption reaction fit pseudo 2nd order kinetic model and the adsorption process can be regulated by the chemisorptions process.

##### Elovich Model

Figure 14c depicts Elovich model fitting. The calculated parameters for Elovich, ( $\alpha$ ,  $\beta$ ) in Table 2 show that the

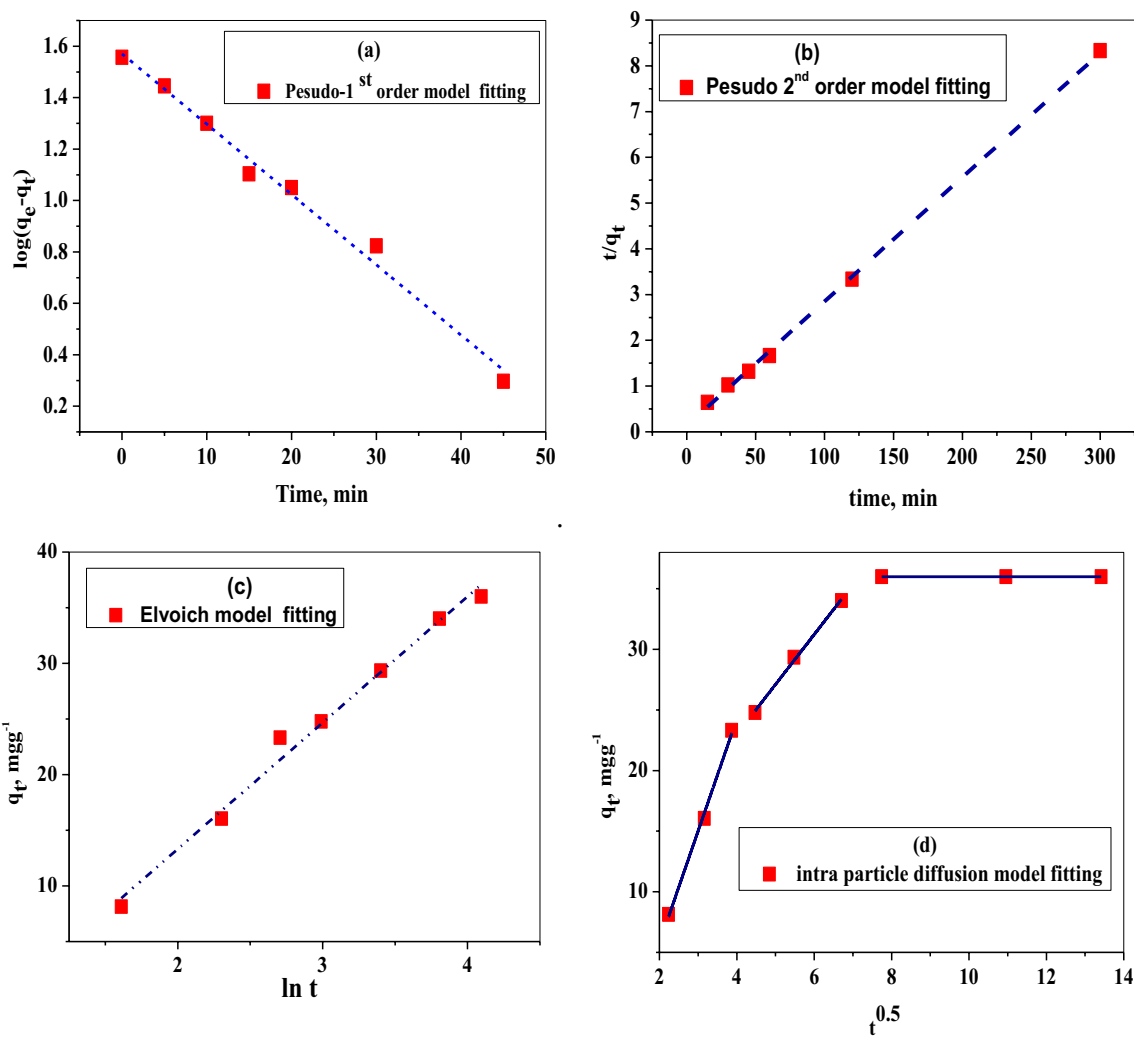


Fig. 14 Kinetic modelling fitting plot for the sorption of rare earth ions onto P(AA-co-AM/PJM-T) at 25 °C and initial concentration 200 mg l<sup>-1</sup>

Table 2 The values of parameters of Kinetic models fitting for rare earth ions sorption onto P (AA-co-AM/PJM-T) composite at 25 °C

Pseudo 1st order kinetic fitting parameters			Pseudo 2nd order kinetic fitting parameters			q <sub>e (exp)</sub> mg g <sup>-1</sup>	Elvoich model fitting parameters		
k <sub>1</sub> , min <sup>-1</sup>	q <sub>e(calc.)</sub> mg g <sup>-1</sup>	R <sup>2</sup>	K <sub>2</sub> gmg <sup>-1</sup> min <sup>-1</sup>	Q <sub>e(calc.)</sub> mg g <sup>-1</sup>	R <sup>2</sup>		α	β	R <sup>2</sup>
0.0623 ± 4.9 × 10 <sup>-3</sup>	37.17 ± 2.57	0.98	0.063 ± 3.15 × 10 <sup>-3</sup>	36.83 ± 0.891	0.99	36	4.966	0.088 ± 0.53	0.98

sorption reaction mechanism can be interpreted by Elovich equation. The correlation factor (R<sup>2</sup>) is greater than 0.98. The data shows that Elovich model involves chemisorptions of the prepared composite toward rare earth ions ensure pseudo 2nd order model.

Table 3 The value of parameters of intra-particle for rare earth ions sorption onto P(AA-co-AM/PJM-T) composite at 25 °C

Intra-particle diffusion model fitting parameters			
Time range, min	K <sub>di</sub> , g mg <sup>-1</sup> min <sup>-1</sup>	C	R <sup>2</sup>
0–15	9.253 ± 0.49	-12.75 ± 1.54	0.99
20–45	4.121 ± 0.21	6.498 ± 1.18	0.99
60–120	–	36	–

**Intra-particle Diffusion Model**

The relation between  $q_t$  and  $t^{1/2}$  for the adsorption of rare earth ions belongs to the intra particle diffusion fitting, Fig. 14d the straight lines with intercept i.e. not crossing the origin point; this means that the film diffusion mechanism is dominated during this study.

The thickness of the surface extrapolated from the intercept describes the participation of the surface adsorption within the rate-determining step. The great value of the intercept, the greater is its participation. It's obvious that the intra-particle diffusion kinetic model for the rare earth adsorption reaction occurred through 3 stages. The primary stage (0–15 min) is that the mass transfer of rare earth ions and this occurs instantaneously and this stage

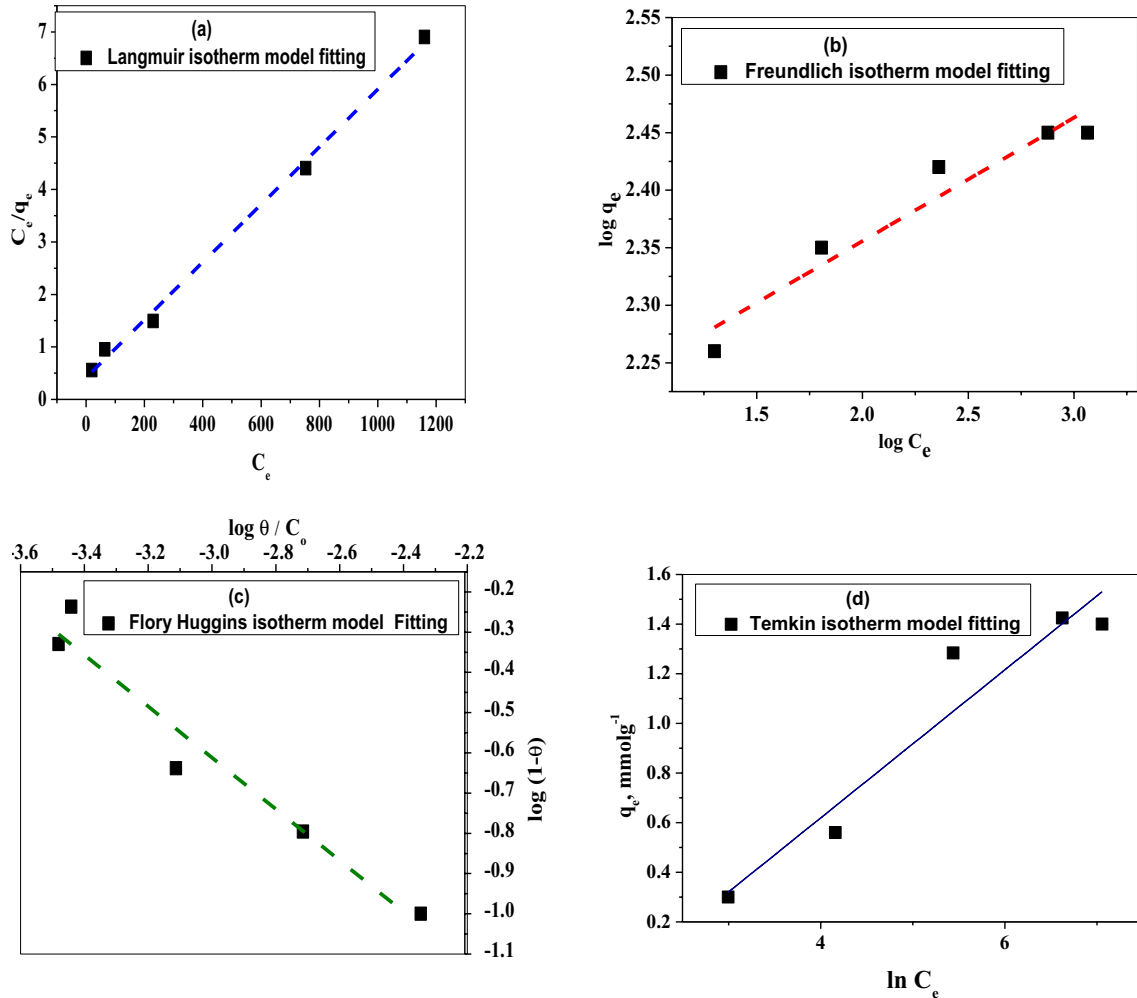


**Fig. 15** Isotherm modelling fitting plot for the sorption of rare earth ions onto P(AA-co-AM/PJM-T) at 25 °C

**Table 4** The values of parameters of equilibrium isotherm models fitting for rare earth ions sorption onto P(AA-co-AM/PJM-T) composite at 25 °C

Langmuir isotherm model				Freundlich isotherm model			Flory–Huggins isotherm model			Temkin isotherm model		
$Q_o$ ( $\text{mgg}^{-1}$ )	$b$ ( $\text{L mg}^{-1}$ )	$R_L$	$R^2$	$K_F$ ( $\text{mgg}^{-1}$ )	$n$	$R^2$	$K_{FH}$	$n_{FH}$	$R^2$	$A_t$	$b_t$ $\text{kJmol}^{-1}$	$R^2$
182.15 $\pm 3.73$	0.0131 $\pm 2.5 \times 10^{-3}$	0.295	0.995	$138.48 \pm 12.83$	$9.33 \pm 8.1$	0.91	$2.97 \times 10^{-3}$	$0.638 \pm 0.08$	0.94	0.146	8.305	0.90
$\Delta G^\circ = RT \ln K_{FH} - 14.393 \text{ kJmol}^{-1}$												

is not considered by the kinetic. The second stage from (20–60 min; is the film diffusion of the rare earth ions from the solution to the surface of the composite and this the rate determining step. The third one (from 60 to 100 min) is that the equilibrium saturation. Table 3 shows the coefficients calculated from the second part of the linear plot.

## Isotherm Modeling

### Langmuir Isotherm Modeling

The relation of Langmuir isotherm and its calculated parameters are shown in Fig. 15a and Table 4, respectively. The linear relation with correlation factor ( $R^2=0.995$ ) assumes the applicability of the sorption process to Langmuir model. The monolayer adsorption capacity at 25 °C and pH 4.5 is  $182.15 \pm 3.73 \text{ mg g}^{-1}$ . Furthermore, the value of  $R_L$  shows in Table 4, 0.295 is more than 0 and less than 1. This implies that, the sorption reaction of rare earth ions onto P (AA-co-AM/PJM-T) at 25 °C is favourable.

### Freundlich Isotherm Modeling

Applying Freundlich Eq. (8). The linear plot in Fig. 15b indicates a probability for the sorption reaction fitting to Freundlich. The calculated parameters for Freundlich isotherm in Table 4 clarify that the value of  $1/n$  is not up to unity; this means that, the sorption process is concentration dependent. The values of correlation coefficient  $R^2$ , (0.91) are less than that of the Langmuir model (0.995); thus, Langmuir isotherm is more regulated for the sorption process.

### Flory–Huggins Isotherm Modelling

Figure 15c represents the graphical representation of Flory–Huggins model and the obtained characteristic constants values of this model are presented in Table 4.  $\Delta G^\circ$  calculated using the values of the equilibrium constant  $K_{FH}$ ; and found to be  $-14.393 \text{ kJ/mol}$  indicates a spontaneous nature of the sorption process.

### Temkin Isotherm Modeling

$A_T$  and  $B_T$  depicted from the intercept and the slope of the plot applying Temkin Eq. (13) in Fig. 15d. The data illustrated in Table 4, indicate that  $b_T$ , is  $8.305 \text{ kJmol}^{-1}$  which confirm chemical adsorption. Value of correction factor ( $R^2$ ) is (0.9) which gives a probability for regulation with the model.

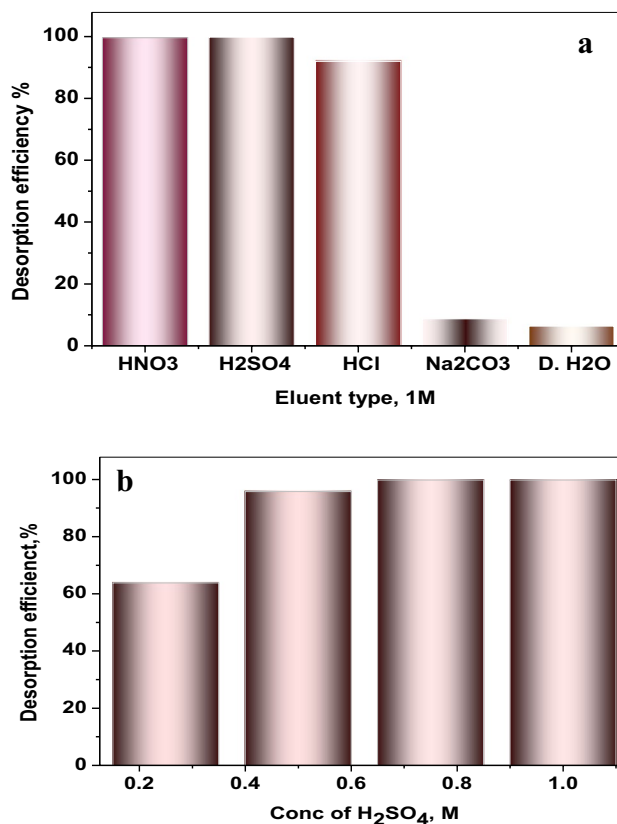
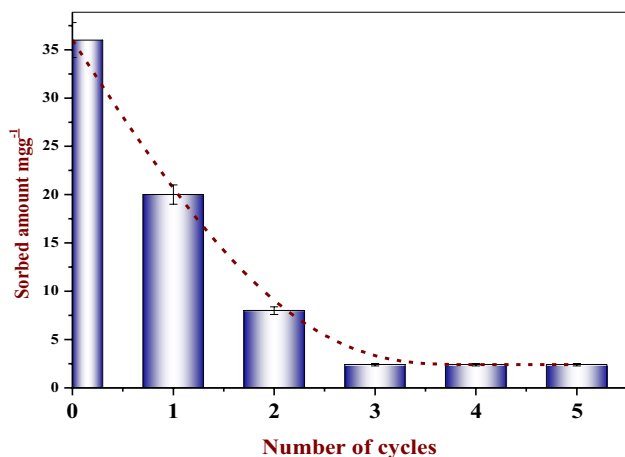


Fig. 16 Desorption study a using different eluents b different concentrations of  $\text{H}_2\text{SO}_4$

## Desorption studies

Desorption process is an important process to low the cost and decrease the need to continual supply of the adsorbent. Thus, the more desorption percentage is the more efficient process and a remark or the good sorbent [55]. The desorption efficiency was studied (Fig. 16a). For  $\text{HNO}_3$ ,  $\text{H}_2\text{SO}_4$ ,  $\text{HCl}$ ,  $\text{Na}_2\text{CO}_3$  and distilled  $\text{H}_2\text{O}$ . The desorption efficiencies of sorbed rare earth ions is in the order  $\text{H}_2\text{SO}_4 > \text{HNO}_3 > \text{HCl} > \text{Na}_2\text{CO}_3 > \text{H}_2\text{O}$ , this may due to lanthanide contraction [56] and the affinity of the composite for  $\text{RE}^{3+}$  is effected by pH. The  $\text{pH}_{\text{pzc}}$  of the P(AA-co-AM/PJM-T) composite is 3. This means the surface charge is positive at  $\text{pH} < 3$  and surface affinity to  $\text{RE}^{3+}$  decrease due to repulsion [57]. The  $K_a$  value of the acids is in the order  $\text{HCl} > \text{H}_2\text{SO}_4 > \text{HNO}_3 > \text{H}_2\text{O}$ ,  $\text{Na}_2\text{CO}_3$  is a strong alkaline compound. Exception for the desorption efficiency using  $\text{HCl}$  due to common ion of  $\text{Cl}^-$  and use of  $\text{HCl}$  in dissolving of the digested  $\text{RE}^{3+}$  hydroxide in caustic soda process. Considering the economy,  $\text{H}_2\text{SO}_4$  is chosen for desorption process.

Desorption processes with  $\text{H}_2\text{SO}_4$  (Fig. 16b) has been worked using various concentrations 0.25, 0.5, 0.75 and 1 M. Among these concentrations 0.75 M shows desorption



**Fig. 17** Reusability of P(AA-co-AM/PJM-T) composite for adsorption of RE<sup>3+</sup> using [H<sub>2</sub>SO<sub>4</sub>]=0.75 M

efficiency percent 99.8% equal to 1 M concentration. As the concentration of [H<sup>+</sup>] increases, H<sup>+</sup> compete RE<sup>3+</sup> and ion exchange takes place. So, it's recommended to use 0.75 M H<sub>2</sub>SO<sub>4</sub> as an eluent for P(AA-co-AM/PJM-T)/RE ion desorption.

### Regeneration of the Adsorbent

The adsorbent synthesis or the sorption process cost can be minimized by effectively reusability of adsorbent materials. As a result, in real applications, the estimation of adsorbent stability and reusability is critical. For assessing the practical application of P(AA-co-AM/PJM-T) composite, we evaluated its reusability by recovering REEs from the prepared stock solution followed by REE release and sorbent

**Table 5** Sorption efficiency of RE<sup>3+</sup> onto P(AA-co-AM/PJM-T) for 24 h at 25 °C by (ICP-OES)

Element	Sorption efficiency (%)
La	87.2 ± 4.36
Ce	84.11 ± 4.21
Pr	81.22 ± 4.061
Nd	82.57 ± 4.13
Sm	87.4 ± 4.37
Eu	95.2 ± 4.76
Gd	84.3 ± 4.215
Tb	84.17 ± 8.417
Dy	84.94 ± 4.247
Ho	83.1 ± 4.155
Er	82.8 ± 4.14
Tm	84.3 ± 4.215
Yb	93.8 ± 4.69
Lu	77.7 ± 3.885

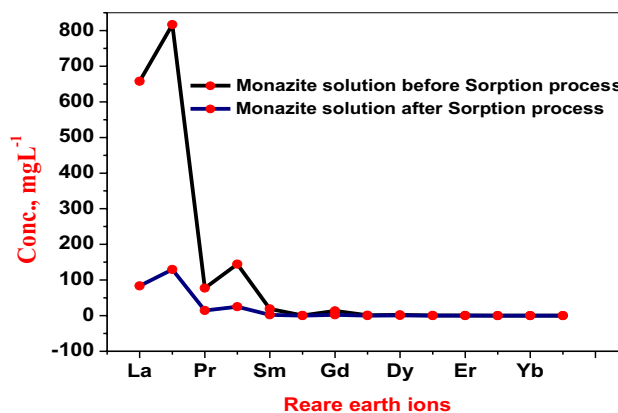


**Fig. 18** Concentration of rare earth ions (RE<sup>3+</sup>) liquor produced from monazite before and after sorption onto P(AA-co-AM/PJM-T) composite at 25 °C

regeneration. The desorption agent in this investigation was 0.75 M H<sub>2</sub>SO<sub>4</sub> solution, and the desorption time was 1 h. The reusability performance (adsorption–desorption–adsorption) was depicted in Fig. 17. The sorption capacity of P(AA-co-AM/PJM-T) composite decreased after the first cycle from 36 mg g<sup>-1</sup> to 20 mg g<sup>-1</sup>. After second cycle, the sorption capacity decreased from 20 mg g<sup>-1</sup> to 8 mg g<sup>-1</sup> then further decrease to 2.4 mg g<sup>-1</sup> in the third cycle. The sorption capacity did not change in the subsequent cycles fourth and fifth cycle. It can be inferred that both ion exchange and the covalent bonding between metal ions and composite play a role in the adsorption process.

### Real Application

Concentration of rare earth ions (RE<sup>3+</sup>) liquor produced from monazite digestion is measured before sorption process with the aid of Ion coupled plasma. The result illustrated in Table 5. The concentration of (RE<sup>3+</sup>) after sorption process is measured by shaking 20 ml of the liquor digested solution for 24 h at 25 °C with 0.1 g of P(AA-co-AM/PJM-T) and pH adjusted at 4.5. The sorption efficiency of RE<sup>3+</sup> onto P(AA-co-AM/PJM-T) is shown in Table 5 and illustrated in Fig. 18. The results are confirmed by the energy dispersive X-ray spectra of loaded P(AA-co-AM/PJM-T) composite with REEs (Fig. 19a). Beside Carbon, nitrogen and oxygen bands, the main constituents of P(AA-co-AM/PJM-T), the spectrum shows La, Ce, Nd, Pr, Sm, Gd, Yb, and Er, Dy bands besides Si, Cl, Ca and Al consistent with the elemental formula of monazite [58].

The roughness of the surface of P(AA-co-AM/PJM-T) becomes rough at the end of the sorption processes as depicted in Fig. 19b. Furthermore, the mapping images of loaded P(AA-co-AM/PJM-T) composite with REEs indicate that REEs ions are adequately adsorbed at the surface of the

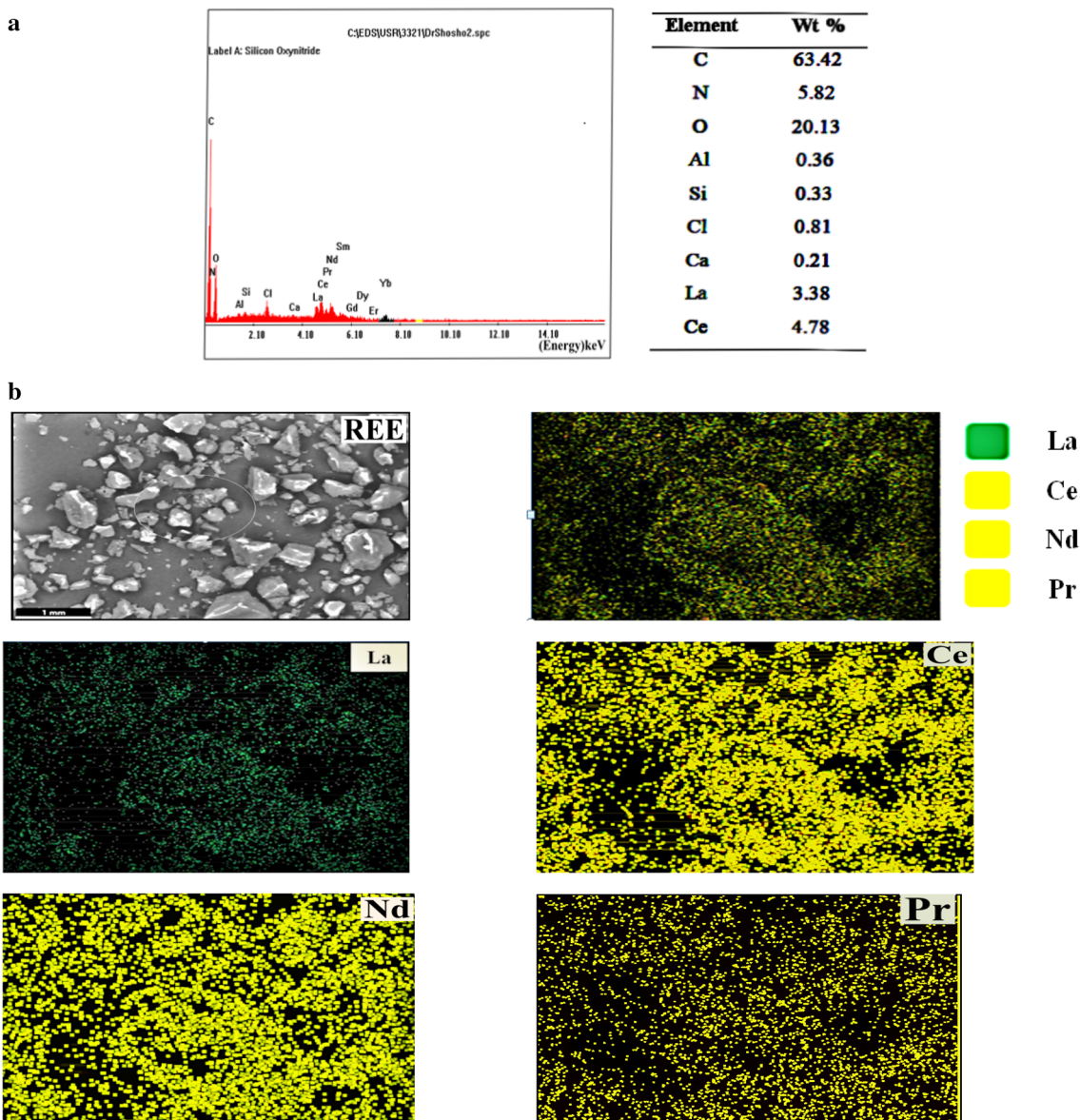


**Fig. 19** **a** EDX spectra of loaded P(AA-co-AM/PJM-T) composite with REEs after contacting with liquor produced from monazite digestion for 24 h. **b** SEM of loaded P(AA-co-AM/PJM-T) composite with REEs after contacting with liquor produced from monazite digestion for 24 h

composite and they are distributed uniformly. La, Ce, Nd, and Pr are taken as examples of REEs to confirm sorption process.

### Comparison with Other Adsorbents

There are several adsorbents that are used for  $RE^{3+}$  sorption from different minerals [59–65]. Compared the maximum sorption capacity ( $q_{max}$ ) of other  $RE^{3+}$  adsorbents with ( $q_{max}$ ) of the P(AA-co-AM/PJM-T) adsorbent is listed in Table 6. It was observed that the adsorption capacity of P(AA-co-AM/PJM-T) adsorbent has reasonable adsorption capacities of  $182.15 \pm 3.73 \text{ mg g}^{-1}$  for  $RE^{3+}$ . Thus, P(AA-co-AM/PJM-T)

showed high potential for sorption of  $RE^{3+}$  could be used for recovery of REE from its ores.

### Conclusion

Poly (acrylic acid-co-acrylamide/16, 16-dimethylheptadecan-1-amine) [P (AA-co-AM/PJM-T)] was successfully copolymerized using gamma irradiation with  $^{60}Co$   $\gamma$ -rays at a dose of 25 KGy. The prepared composite characterized by several physic chemical methods and its applicability for adsorbing REEs elements from acidic aqueous solutions was investigated. The best adsorption parameters at



**Table 6** Comparison of maximum adsorption capacity of adsorbents reported in literature for REEs

Adsorbent	pH	$q_{\max}$	References
Polystyrene-poly(hydroxamic Acid) copolymer at 40 °C			[59]
La <sup>3+</sup>	2	1.27 m mol g <sup>-1</sup>	
Ce <sup>3+</sup>	1	1.53 m mol g <sup>-1</sup>	
Y <sup>3+</sup>	3	1.83 m mol g <sup>-1</sup>	
Walnut shell	4	6.5–8 mg g <sup>-1</sup>	[60]
Natural polymers thiourea functionalized cellulose			[61]
Eu (III)	–	27 mg g <sup>-1</sup>	
Nd (III)		73 mg g <sup>-1</sup>	
Metal–organic framework (MOF), HKUST-1	6	234 mg g <sup>-1</sup>	[62]
Ce <sup>3+</sup>		203 mg g <sup>-1</sup>	
La <sup>3+</sup>			
Biosorbents			[63]
1		29.16 mg g <sup>-1</sup>	
2	4.24	31.91 mg g <sup>-1</sup>	
3		34.53 mg g <sup>-1</sup>	
EDTA-functionalized activated carbon		71.42 mg g <sup>-1</sup>	[64]
EDTA functionalized magnetic and nonmagnetic nanoparticles		100–400 mg g <sup>-1</sup>	[65]
magnetic mesoporous Fe <sub>3</sub> O <sub>4</sub> @mSiO <sub>2</sub> –DODGA nanoparticles		367 μ mg g <sup>-1</sup>	[66]
P(AA-co-AM/PJM-T)	4.5	182.15 ± 3.73 mg g <sup>-1</sup>	This study

25 °C of REEs ions are; 0.1 g [P (AA-co-AM/PJM-T)] with 20 ml REE ions solution, contact time 60 min, pH=4.5. Kinetic and isotherm models applied. The results indicated that, the sorption reaction is regulated by pseudo 2nd order model than pseudo 1st order model. The adsorption mechanism was checked for Langmuir, Freundlich, Flory–Huggins and Temkin isotherm models. Langmuir adsorption capacity of rare earth ions onto P(AA-co-AM/PJM-T) is 182.15 ± 3.73 mg g<sup>-1</sup>. P(AA-co-AM/PJM-T) applied on liquor solution of the digested monazite with total concentration of for rare earth ions 1608 mg L<sup>-1</sup> and the sorption efficiencies (%) of the single ions range from 95.2% for Eu<sup>3+</sup> and 77.7% for Lu<sup>3+</sup>. Thus, [P (AA-co-AM/PJM-T)] is high selective for REEs.

**Author Contributions** All authors contributed to the study conception and design, Material preparation, data collection and analysis. All authors read and approved the final manuscript.

**Funding** The authors received no financial support for the research, authorship, and/or publication of this article.

**Data Availability** All the data used for this work are publicly available.

## Declarations

**Conflict of interest** The authors declare that they have no conflict of interest.

**Ethical Approval** The authors confirm that the manuscript has been read and approved by all authors. The authors declare that this manu-

script has not been published and not under consideration for publication elsewhere.

**Consent to Participate** All of the authors consented to participate in the drafting of this manuscript.

**Consent for Publication** All of the authors consent to publish this manuscript.

**Research Involving Human Participants and/or Animals** Not applicable.

## References

- An F, Gao B, Huang X, Zhang Y, Li Y, Xu Y, Zhang Z, Gao J, Chen Z (2013) Selectively removal of Al (III) from Pr(III) and Nd(III) rare earth solution using surface imprinted polymer. *React Funct Polym* 73(1):60–65. <https://doi.org/10.1016/j.reactfunctpolym.2012.08.022>
- Celik I, Kara D, Karadas C, Fisher A, Hill SJ (2015) A novel ligandless-dispersive liquid–liquid microextraction method for matrix elimination and the preconcentration of rare earth elements from natural waters. *Talanta* 134:476–481. <https://doi.org/10.1016/j.talanta.2014.11.063>
- Unal YS, Eroglu AE, Shahwan T (2013) Removal of aqueous rare earth elements (REEs) using nano-iron based materials. *J Ind Eng Chem* 19:898–907. <https://doi.org/10.1016/j.jiec.2012.11.005>
- Yon H, Kim C, Chung K, Kim S, Lee J, Kumar JR (2016) Solvent extraction, separation and recovery of dysprosium (Dy) and neodymium (Nd) from aqueous solutions: waste recycling strategies for permanent magnet processing. *Hydrometallurgy* 165(1):27–43. <https://doi.org/10.1016/j.hydromet.2016.01.028>
- Parhi PK, Park KH, Nam CW, Park JT (2015) Liquid–liquid extraction and separation of total rare earth (RE) metals from polymetallic manganese nodule leaching solution. *J Rare Earths* 33:207–213. [https://doi.org/10.1016/S1002-0721\(14\)60404-X](https://doi.org/10.1016/S1002-0721(14)60404-X)

6. Ashour RM, Abdel-Magied AF, Abdel-khalek AA, Helaly OS, Ali MM (2016) Preparation and characterization of magnetic iron oxide nanoparticles functionalized by L-cysteine: adsorption and desorption behavior for rare earth metal ions. *J Environ Chem Eng* 4:3114–3121. <https://doi.org/10.1016/j.jece.2016.06.022>
7. Ashour RM, El-sayed R, Abdel-Magied AF, Abdel-khalek AA, Ali MM, Forsberg K, Uheida A, Muhammed M, Dutta J (2017) Selective separation of rare earth ions from aqueous solution using functionalized magnetite nanoparticles: kinetic and thermodynamic studies. *Chem Eng J* 327:286–296. <https://doi.org/10.1016/j.cej.2017.06.101>
8. Gok C (2014) Neodymium and samarium recovery by magnetic nano-hydroxyapatite. *J Radioanal Nucl Chem* 301:641–651. <https://doi.org/10.1007/s10967-014-3193-z>
9. Liang P, Liu Y, Guo L (2005) Determination of trace rare earth elements by inductively coupled plasma atomic emission spectrometry after preconcentration with multiwalled carbon nanotubes. *Spectrochim Acta B* 60:125–129. <https://doi.org/10.1016/j.sab.2004.11.010>
10. Goodenough KM, Wall F, Merriman D (2018) The rare earth elements: demand, global resources, and challenges for resourcing future generations. *Nat Resour Res* 27:201
11. Lima AT, Ottosen L (2021) Recovering rare earth elements from contaminated soils: critical overview of current remediation technologies. *Chemosphere* 265:129163. <https://doi.org/10.1016/j.chemosphere.2020.129163>
12. Tianchi L, Ji C (2021) Extraction and separation of heavy rare earth elements (2021) a review. *Sep Purif Technol* 276:119263. <https://doi.org/10.1016/j.seppur.2021.119263>
13. Quijada-Maldonado E, Romero J (2021) Solvent extraction of rare-earth elements with ionic liquids: toward a selective and sustainable extraction of these valuable elements. *Curr Opin Green Sustain Chem* 27:2452–2236. <https://doi.org/10.1016/j.cogsc.2020.100428>
14. Ang KL, Li D, Nikoloski AN (2017) The effectiveness of ion exchange resins in separating uranium and thorium from rare earth elements in acidic aqueous sulfate media. Part 1. Anionic and Cationic Resins *Hydrometall* 174:147–155
15. Elkhansa E, Afnan M, MhdAmmar H, Alaa H (2021) Recovery of rare earth elements from waste streams using membrane processes: an overview. *Hydrometallurgy* 204:105706. <https://doi.org/10.1016/j.hydromet.2021.105706>
16. Xu X, Jiang X, Jiao F, Chen X, Yu J (2018) Tunable assembly of porous three-dimensional graphene oxide-corn zein composites with strong mechanical properties for adsorption of rare earth elements. *J Taiwan Inst Chem Eng* 85:106–114
17. Gupta NK, Gupta A, Ramteke P, Sahoo H, Sengupta A (2019) Biosorption—a green method for the preconcentration of rare earth elements (REEs) from waste solutions: a review. *J Mol Liq* 274:48–164. <https://doi.org/10.1016/j.molliq.2018.10.134>
18. Veliscek-Carolan J, Jolliffe K, Hanley T (2013) Selective sorption of actinides by Titania nanoparticles covalently functionalized with simple organic ligands. *Appl Mater Interfaces* 5(22):11984–11994. <https://doi.org/10.1021/am403727x>
19. Desouky OA, Daher AM, Abdel-Monem YK, Galhoum AA (2009) Liquid–liquid extraction of yttrium using primene-JMT from acidic sulfate solutions. *Hydrometallurgy* 96(4):313–317. <https://doi.org/10.1016/j.hydromet.2008.11.009>
20. Janczura M, Luliński P, Sobiech M (2021) Imprinting technology for effective sorbent fabrication: current state-of-art and future prospects. *Materials* 14(8):1850. <https://doi.org/10.3390/ma14081850>
21. García-Otero N, Teijeiro-Valiño C, Otero-Romaní J, Peña-Vázquez E, Moreda-Piñeiro A, Bermejo-Barrera P (2009) On-line ionic imprinted polymer selective solid-phase extraction of nickel and lead from seawater and their determination by inductively coupled plasma-optical emission spectrometry. *Anal Bioanal Chem* 395(4):1107–1115. <https://doi.org/10.1007/s00216-009-3044-x>
22. Li-pan JIA, Jiang-kiang H, Ze-long MA, Xu-heng LIU, Xing-yu C, Jiang-tao LI, Li-hua HE, Zhong-wei Z (2020) Research and development trends of hydrometallurgy: an overview based on hydrometallurgy literature from 1975 to 2019. *Trans Nonferrous Metals Soc China* 30(11):1003–6326. [https://doi.org/10.1016/S1003-6326\(20\)65450-4](https://doi.org/10.1016/S1003-6326(20)65450-4)
23. Han Z, Xiao-Kun O, Li-Ye Y (2021) Adsorption of lead ions from aqueous solutions by porous cellulose nanofiber–sodium alginate hydrogel beads. *J Mol Liq* 324:115122. <https://doi.org/10.1016/j.molliq.2020.115122>
24. Xu X, Ouyang X, Yang LY (2020) Adsorption of Pb (II) from aqueous solutions using crosslinked carboxylated chitosan/carboxylated nanocellulose hydrogel beads. *J Mol Liq*. <https://doi.org/10.1016/j.molliq.2020.114523>
25. Zhang H, Omer AM, Hu Z, Yang LY, Ji C, Ouyang X (2019) Fabrication of magnetic bentonite/carboxymethyl chitosan/sodium alginate hydrogel beads for Cu (II) adsorption. *Int J Biol Macromol* 135:490–500. <https://doi.org/10.1016/j.ijbiomac.2019.05.185>
26. Wang X, Wang A (2010) Adsorption characteristics of chitosan-g-Poly (acrylic acid) hydrogel composite for Hg (II) ions from aqueous solution. *Sep Sci Technol* 45:2086–2094
27. Rivas BL, Peric IM, Munoz C, Alvear R (2011) Poly (N-hydroxymethyl acrylamide-co-acrylic acid) and poly (N-hydroxymethyl acrylamide-co acrylamidoglycolic acid): synthesis, characterization, and metal ion removal properties. *Polym Bull* 68:391–403. <https://doi.org/10.1007/s00289-011-0551-7>
28. Guclu G, Al E, Emik S, Iyim TB, Ozgumus S, Ozyurek M (2010) Removal of Cu<sup>2+</sup> and Pb<sup>2+</sup> ions from aqueous solutions by starch-graft-acrylic acid/montmorillonite superabsorbent nanocomposite hydrogels. *Polym Bull* 65:333–346. <https://doi.org/10.1007/s00289-009-0217-x>
29. Cavus S, Gurdag G, Sozgen K, Gurkaynaka MA (2009) The preparation and characterization of poly (acrylic acid-co-methacrylamide) gel and its use in the non-competitive heavy metal removal. *Polym Adv Technol* 20:165–172. <https://doi.org/10.1002/pat.1248>
30. Wei J, Xiao Y, Yang C, Cai Y, Luo W, Luo T, Li H, Yang Z (2021) Dense polyacrylic acid-immobilized polypropylene non-woven fabrics prepared via UV-induced photo graft technique for the recovery of rare earth ions from aqueous solution. *J Polym Environ*. <https://doi.org/10.1007/s10924-021-02068-8>
31. Attallah MF, Allan KF, Mahmoud MR (2016) Synthesis of poly (acrylic acid–maleic acid) SiO<sub>2</sub>/Al<sub>2</sub>O<sub>3</sub> as novel composite material for cesium removal from acidic solutions. *J Radioanal Nucl Chem* 307(2):1231–1241
32. Vincent B, Julien M, Alain G, Xianyu D, Jean-Jacques R, Sophie M (2020) Acidic polymeric sorbents for the removal of metallic pollution in water: a review. *React Funct Polym* 152:104599. <https://doi.org/10.1016/j.reactfunctpolym.2020.104599>
33. Cheremisinoff P (1997) Handbook of engineering polymeric materials, 1st edn. CRC Press, Boca Raton. <https://doi.org/10.1201/9781482292183>
34. Heidari S, Esmailzadeh F, Mowla D, Ghasemi S (2018) Synthesis of an efficient copolymer of acrylamide and acrylic acid and determination of its swelling behavior. *J Petrol Explor Prod Technol* 8:1331–1340. <https://doi.org/10.1007/s13202-017-0428-x>
35. Labib SH, Shahr El-Din AM, Allan KF, Attallah MF (2020) Synthesis of highly deficient nano SrCoO<sub>x</sub> for the purification of lanthanides from monazite concentrate. *J Radioanal Nucl Chem* 323:1179–1188. <https://doi.org/10.1007/s10967-020-07031-w>
36. Hassan HS, Attia Lamis A, Dakrouy GA (2020) Exploration of the parameters affecting the radioactive europium removal from aqueous solutions by activated carbon-epoxy composite. *Appl Radiat Isot* 164:109278. <https://doi.org/10.1016/j.apradiso.2020.109278>

37. Lagergren S (1898) About the theory of so-called adsorption of soluble substance. *Kungliga Svenska Vetenskaps-Akademiens Handlingar* 24:1–39
38. McKay G, Ho YS (1999) Pseudo-second order model for sorption processes. *Process Biochem* 34:451–465
39. Cheung CW, Porter JF, McKay G (2000) Sorption kinetics for the removal of copper and zinc from effluents using bone char. *J Sep Purif Technol* 19(1–2):55–64 [https://doi.org/10.1016/S1383-5866\(99\)00073-8](https://doi.org/10.1016/S1383-5866(99)00073-8)
40. Weber WJ, Morris JC (1963) Kinetics of adsorption on carbon from solution. *J Sanit Eng Div Am Soc Civ Eng* 89:31–60
41. Langmuir I (1918) The adsorption of gases on plane surfaces of glass, mica and platinum. *J Am Chem Soc* 40(9):1361–1403. <https://doi.org/10.1021/ja02242a004>
42. Weidner E, Ciesielczyk F (2019) Removal of hazardous oxyanions from the environment using metal-oxide-based. *Materials* 12:927
43. Foo KY, Hameed BH (2010) Review: insights into the modeling of adsorption isotherm systems. *Chem Eng J* 156:2–10
44. Vijayaraghavan K, Padmesh TVN, Palanivelu K, Velan M (2006) Biosorption of nickel(II) ions onto *Sargassum wightii*: application of two-parameter and three-parameter isotherm models. *J Hazard Mater* 133(1–3):304–308
45. Todica M, Razvan S, Pop C, Loredana O (2015) IR and Raman investigation of some poly(acrylic acid) gels in aqueous and neutralized state. *Acta Physica Polonica A* 128:128–135. <https://doi.org/10.1693/APhysPolA.128.128>
46. Shahid SA, Qidwai AA, Anwar F, Ullah I, Rashid U (2012) Improvement in the water retention characteristics of sandy loam soil using a newly synthesized poly(acrylamide-co-acrylic Acid)/AlZnFe<sub>2</sub>O<sub>4</sub> superabsorbent hydrogel nanocomposite material. *Molecules* 17(8):9397–9412. <https://doi.org/10.3390/molecules17089397>
47. Lu Y, Wang Z, Ouyang X, Ji C, Liu Y, Huang F, Yang L (2019) Fabrication of cross-linked chitosan beads grafted by polyethyl-enimine for efficient adsorption of diclofenac sodium from water. *Int J Biol Macromol*. <https://doi.org/10.1016/j.ijbiomac.2019.10.044>
48. Chalal S, Haddadine N, Bouslah N, Benaboura A (2012) Preparation of Poly (acrylic acid)/silver nanocomposite by simultaneous polymerization-reduction approach for antimicrobial application. *J Polym Res*. <https://doi.org/10.1007/s10965-012-0024-1>
49. Moharram M, Mousa A (2007) Study of the interaction of poly (acrylic acid) and poly (acrylic acid-poly acrylamide) complex with bone powders and hydroxyapatite by using TGA and DSC. *J Appl Polym Sci* 105:3220–3227. <https://doi.org/10.1002/app.26267>
50. Xiong C, Liu X, Yao C (2008) Effect of pH on sorption for RE (III) and sorption behaviors of Sm (III) by D152 resin. *J Rare Earths* 26:851–856. [https://doi.org/10.1016/S1002-0721\(09\)60020-X](https://doi.org/10.1016/S1002-0721(09)60020-X)
51. Puigdomenech I (2013) Make equilibrium diagrams using sophisticated algorithms (MEDUSA). In: *Inorganic chemistry*. Royal Institute of Technology, Stockholm, Sweden. <http://www.kemi.kth.se/medusa>. <https://sites.google.com/site/chemdiagr/>
52. HENDY A, Khozamy E, Mahmoud G, Saad E, Serror S (2019) Implementation of carboxymethyl cellulose/acrylic acid/titanium dioxide nanocomposite hydrogel in remediation of Cd(II), Zn(II) and Pb(II) for water treatment application. *Egypt J Chem* 62(10):1785–1798. <https://doi.org/10.21608/ejchem.2019.11622.1739>
53. Akpomie KG, Dawodu FA, Adebowale KO (2015) Mechanism on the sorption of heavy metals from binary-solution by a low cost montmorillonite and its desorption potential. *Alex Eng J* 54:757–767. <https://doi.org/10.1016/j.aej.2015.03.025>ISSN1110-0168
54. Ouyang D, Zhuo Y, Hu L, Zeng Q, Hu Y, He Z (2019) Research on the adsorption behavior of heavy metal ions by porous material Prepared with silicate tailings. *Minerals* 9(5):291. <https://doi.org/10.3390/min9050291>
55. Ponou O, Wang LP, Dobbiba G, Okaya K, Fujita T, Mitsuhashi K, Atarashi T, Satoh G, Noda M (2014) Recovery of rare earth elements from aqueous solution obtained from Vietnamese clay minerals using dried and carbonized parachlorella. *J Environ Chem Eng* 2:1070–1081. <https://doi.org/10.1016/j.jece.2014.04.002>
56. Coppin F, Berger G, Bauer A, Castet S, Loubet M (2002) Sorption of lanthanides on smectite and kaolinite. *Chem Geol* 182:57–68. [https://doi.org/10.1016/S0009-541\(01\)00283-2](https://doi.org/10.1016/S0009-541(01)00283-2)
57. Shan X, Lian J, Wen B (2002) Effect of organic acids on adsorption and desorption of rare earth elements. *Chemosphere* 47(7):701–710
58. Zglinicki K, Szamałek K, Wołkowicz S (2021) Critical minerals from post-processing tailing. A case study from Bangka Island Indonesia. *Minerals* 11(4):352. <https://doi.org/10.3390/min11040352>
59. Cao X, Wang Q, Wang S, Man R (2020) Preparation of a novel polystyrene-poly(hydroxamic acid) copolymer and its adsorption properties for rare earth metal ions. *Polymers* 12(9):1905. <https://doi.org/10.3390/polym12091905>
60. Gallardo K, Castillo R, Mancilla N, Remonsellez F (2020) Biosorption of rare-earth elements from aqueous solutions using walnut shell. *Front Chem Eng*. <https://doi.org/10.3389/fceng.2020.00004>
61. Negrea A, Gabor A, Davidescu CM, Ciopec M, Negrea P, Duteanu N, Barbulescu A (2018) Rare earth elements removal from water using natural polymers. *Sci Rep*. <https://doi.org/10.1038/s41598-017-18623>
62. Zhao L, Duan X, Azhar MR, Sun H, Fang X, Wang S (2020) Selective adsorption of rare earth ions from aqueous solution on metal-organic framework HKUST-1. *Chem Eng J Adv*. <https://doi.org/10.1016/j.cej.2020.100009>
63. Kosheleva A, Atamaniuk I, Politaeva N, Kuchta K (2018) Adsorption of rare earth elements using bio-based sorbents. *MATEC Web Conf* 245:18001. <https://doi.org/10.1051/mateconf/201824518001>
64. Babua C, Binnemans K, Roosen J (2018) EDTA-functionalized activated carbon for the adsorption of rare earths from aqueous solutions. *Ind Eng Chem Res* 57(5):1487–1497. <https://doi.org/10.1021/acs.iecr.7b04274>
65. Dupont D, Brullot W, Bloemen M, Verbiest TM, Binnemans K (2014) Selective uptake of rare earths from aqueous solutions by EDTA functionalized magnetic and nonmagnetic nanoparticles. *ACS Appl Mater Interfaces* 6(7):4980–4988. <https://doi.org/10.1021/am406027y>
66. Li J, Gong A, Li F, Qiu L, Zhang W, Gao G, Liu Y, Li J (2018) Synthesis and characterization of magnetic mesoporous Fe<sub>3</sub>O<sub>4</sub>@mSiO<sub>2</sub>-DODGA nanoparticles for adsorption of 16 rare earth elements. *RSC Adv* 8(68):39149–39161. <https://doi.org/10.1039/c8ra07762b>

**Publisher's Note** Springer Nature remains neutral with regard to jurisdictional claims in published maps and institutional affiliations.